

Low-energy electronic recoil in xenon detectors by solar neutrinos

Jiunn-Wei Chen^{a,1,2,3} Hsin-Chang Chi^{b,4} C.-P. Liu^{c,4} and Chih-Pan Wu^{d1}

¹*Department of Physics and Center for Theoretical Sciences,
National Taiwan University, Taipei 10617, Taiwan*

²*Leung Center for Cosmology and Particle Astrophysics,
National Taiwan University, Taipei 10617, Taiwan*

³*Center for Theoretical Physics, Massachusetts Institute of Technology, Cambridge, MA 02139, USA*

⁴*Department of Physics, National Dong Hwa University, Shoufeng, Hualien 97401, Taiwan*

Abstract

Low-energy electronic recoil caused by solar neutrinos in multi-ton xenon detectors is an important subject not only because it is a source of the irreducible background for direct searches of weakly-interacting massive particles (WIMPs), but also because it provides a viable way to measure the solar pp and ${}^7\text{Be}$ neutrinos at the precision level of current standard solar model predictions. In this work we perform *ab initio* many-body calculations for the structure, photoionization, and neutrino-ionization of xenon. It is found that the atomic binding effect yields a sizable suppression to the neutrino-electron scattering cross section at low recoil energies. Compared with the previous calculation based on the free electron picture, our calculated event rate of electronic recoil in the same detector configuration is reduced by about 25%. We present in this paper the electronic recoil rate spectrum in the energy window of 100 eV - 30 keV with the standard per ton per year normalization for xenon detectors, and discuss its implication for low energy solar neutrino detection (as the signal) and WIMP search (as a source of background).

^a E-mail: jwc@phys.ntu.edu.tw

^b E-mail: hsinchang@mail.ndhu.edu.tw

^c E-mail: cpliu@mail.ndhu.edu.tw

^d E-mail: d01222003@ntu.edu.tw

I. INTRODUCTION

Direct searches of weakly-interacting massive particles (WIMPs), one of the favored dark matter (DM) candidates, have been actively pursued in experimental nuclear and particle physics. Although no concrete evidence of WIMPs has been obtained so far, a large portion of the parameter space (in terms of WIMP mass and their cross section to normal matter) has been ruled out. For example, recent results by the PandaX-II [1] and LUX [2] experiments, both employing xenon detectors, set their best upper limits on the spin-independent WIMP-nucleon cross section: $2.5 \times 10^{-46} \text{ cm}^2$ for a $40 \text{ GeV}/c^2$ WIMP and $2.2 \times 10^{-46} \text{ cm}^2$ for a $50 \text{ GeV}/c^2$ WIMP, respectively.

Using Xenon as a detector has several advantages. It is relatively cheap to obtain, easy to scale up, and having enhanced cross sections when scattered coherently. Therefore there are several next-generation WIMP search proposals — XENON1T [3], LZ [4], and DARWIN [5]— all use xenon as detectors. These are multi-ton scale detectors aiming at improving the current sensitivity in WIMP-nucleon cross section by one order of magnitude with a ton-year exposure (a modest goal) to three orders of magnitude with 200 ton-year exposure (an ambitious goal).

To reach high sensitivity in those experiments, proper background removal is crucial. Direct WIMP searches use nuclear recoil as a signal of WIMP-nucleus collision. However, nuclear recoil due to coherent neutrino-nucleus scattering could fake the signal. This kind of background is hard to shield and forms an irreducible background called “neutrino floor” which limits the ultimate sensitivity the experiments can achieve [6].

Neutrino electron scattering is another type of neutrino background which is in principle reducible, but in practice hard to remove completely in experiments. The DARWIN detector, for example, has only a small chance ($\sim 0.02\%$) to mis-identify an electronic recoil in this process as a nuclear recoil signal. However, the large flux from pp (end-point energy at 420 keV) and ${}^7\text{Be}$ (two discrete energies at 862 and 384 keV) solar neutrinos makes electronic recoils the limiting background to measure the cross section on a nucleon lower than $4 \times 10^{-49} \text{ cm}^2$ for WIMP mass of $40 \text{ GeV}/c^2$.

A very interesting observation made in Ref. [7] is that this very phenomenon of neutrino electron scattering that limits the WIMP detection can be turned into an opportunity to measure low energy solar neutrino flux to high precision. It was found that an integrated pp neutrino rate of 5900 events in the recoil energy window of 2-30 keV can be reached by a 70 ton-year exposure, which provides the required statistics for a 1%-level measurement in the pp neutrino flux [7]. (Note that the Borexino experiment observed only part of the pp [8] and ${}^7\text{Be}$ [9] neutrinos because of a high detection threshold at 50 keV, so its precisions in flux measurements are limited.)

However, as demonstrated in our previous work on germanium detectors [10–12], low-energy

electronic recoil around a few keV starts to deviate from the simple free electron approximation and the improved version by including the stepping of atomic shells. In xenon detectors, one expects a similar and even bigger effect from atomic binding. To address this important issue, we adopt an *ab initio* many-body method: the relativistic random phase approximation (RRPA) [13–15]. We first benchmark our calculations with Xenon structure and photo absorption data, then give a reliable prediction for the low-energy electronic recoil spectrum induced by solar neutrinos.

The organization of this paper is as follows. In Sec. II, we gather the essential formalism for neutrino-ionization of an atom and its corresponding electronic recoil spectrum. In Sec. III, we justify our many-body approach to the xenon atom by showing benchmark results on atomic structure and photoabsorption calculations. Our main results for the electronic recoil spectrum induced by solar neutrinos in multi-ton-scale xenon detectors are presented and discussed in Sec. IV. Then we summarize in Sec. V.

II. GENERAL FORMALISM

To calculate the differential cross section for neutrino-ionization of xenon atoms, caused by the weak neutrino-electron interactions, we follow the general formalism described in Ref. [10–12]. In the massless limit of neutrinos $m_\nu \rightarrow 0$, the differential cross section with respect to the energy deposition, denoted as T , by the incoming neutrino of flavor i , is

$$\begin{aligned} \frac{d\sigma^{(i)}}{dT} = & \frac{G_F^2}{\pi} (E_\nu - T)^2 \int d\cos\theta \cos^2\frac{\theta}{2} \left\{ R_{00}^{(i)} - \frac{T}{|\vec{q}|} R_{03+30}^{(i)} + \frac{T^2}{|\vec{q}|^2} R_{33}^{(i)} \right. \\ & \left. + \left(\tan^2\frac{\theta}{2} - \frac{q^2}{2|\vec{q}|^2} \right) R_{11+22}^{(i)} + \tan\frac{\theta}{2} \sqrt{\tan^2\frac{\theta}{2} - \frac{q^2}{|\vec{q}|^2}} R_{12+21}^{(i)} \right\} \end{aligned} \quad (1)$$

in the laboratory frame, where G_F is the Fermi constant; E_ν the incident neutrino energy; θ the neutrino scattering angle; and q (\vec{q}) the 4- (3-) momentum transfer of the neutrino, respectively. The atomic weak response functions

$$\begin{aligned} R_{\mu\nu}^{(i)} = & \frac{1}{2J_i + 1} \sum_{M_{J_i}} \sum_f \langle \Psi_f | c_V^{(i)} \hat{\mathcal{J}}_\mu - c_A^{(i)} \hat{\mathcal{J}}_{5\mu} | \Psi_i \rangle \langle \Psi_f | c_V^{(i)} \hat{\mathcal{J}}_\nu - c_A^{(i)} \hat{\mathcal{J}}_{5\nu} | \Psi_i \rangle^* \\ & \times \delta(T + E_i - E_f), \end{aligned} \quad (2)$$

with Lorentz indices $\mu, \nu = 0, 1, 2, 3$ (the 3-axis is defined by the direction of \vec{q}) involve a sum of the final atomic states $|\Psi_f\rangle$ and a spin average of the initial atomic states $|\Psi_i\rangle = |J_i, M_{J_i}, \dots\rangle$, and the Dirac delta function imposes energy conservation. The (axial-) vector current operator for an electron field $\hat{\psi}_e$ is represented in momentum space

$$\hat{\mathcal{J}}_{\mu(5)} \equiv \int d^3x e^{i\vec{q}\cdot\vec{x}} \hat{\psi}_e(\vec{x}) \gamma^\mu (\gamma_5) \hat{\psi}_e(\vec{x}). \quad (3)$$

TABLE I. The single-particle energies of a Xe atom calculated by DHF (s.p.) in this work versus the edge energies extracted from photoabsorption data (edge) in Ref. [17] (The one for the K -shell is not available). All energies are in units of eV.

	$K(1s_{\frac{1}{2}})$	$L_I(2s_{\frac{1}{2}})$	$L_{II}(2p_{\frac{3}{2}})$	$L_{III}(2p_{\frac{1}{2}})$	$M_I(3s_{\frac{1}{2}})$	$M_{II}(3p_{\frac{3}{2}})$	$M_{III}(3p_{\frac{1}{2}})$	$M_{IV}(3d_{\frac{5}{2}})$	$M_V(3d_{\frac{3}{2}})$
s.p.	34759.3	5509.8	5161.5	4835.6	1170.5	1024.8	961.2	708.1	694.9
edge	-	5452.8	5103.7	4782.2	1148.7	1002.1	940.6	689.0	676.4
	$N_I(4s_{\frac{1}{2}})$	$N_{II}(4p_{\frac{3}{2}})$	$N_{III}(4p_{\frac{1}{2}})$	$N_{IV}(4d_{\frac{5}{2}})$	$N_V(4d_{\frac{3}{2}})$	$O_I(5s_{\frac{1}{2}})$	$O_{II}(5p_{\frac{1}{2}})$	$O_{III}(5p_{\frac{3}{2}})$	
s.p.	229.4	175.6	162.8	73.8	71.7	27.5	13.4	12.0	
edge	213.2	146.7	145.5	69.5	67.5	23.3	13.4	12.1	

Depending on the flavor of the incident neutrino, the vector and axial-vector coupling constants are

$$c_V^{(i)} = -\frac{1}{2} + 2 \sin^2 \theta_w + \delta_{i,e}, \quad c_A^{(i)} = -\frac{1}{2} + \delta_{i,e}, \quad (4)$$

where θ_w is the Weinberg angle; and the difference between ν_e and $\nu_{\mu,\tau}$ is because the former scattering involves both the charged and neutral weak interactions, while the latter is purely neutral.

The differential electronic recoil spectrum induced by a neutrino source is calculated by folding the above differential cross sections $d\sigma^{(i)}(T, E_\nu)/dT$ with the incident neutrino energy spectrum $d\phi^{(i)}(E_\nu)/dE_\nu$:

$$\frac{dN_e(E_e)}{dT} = N_0 \times t \times \sum_{i=e,\mu,\tau} \int dE_\nu \frac{d\phi^{(i)}(E_\nu)}{dE_\nu} \frac{d\sigma^{(i)}(E_e, E_\nu)}{dT}. \quad (5)$$

We shall adopt the standard per-ton per-year per-keV normalization, so the total number of atoms $N_0 = 6.02 \times 10^{29}/A$ (A is the atomic mass of the detector atom in atomic units), t is one year, and energy is measured in units of keV.

III. BENCHMARK CALCULATIONS OF THE XENON ATOM

The atomic many-body wave functions for the initial and final states are computed by an *ab initio* method: the relativistic random phase approximation (RRPA) [13–15].* Because the atomic number of xenon, $Z = 54$, is large, both the relativistic effect and residual two-electron correlation are important. Therefore, the RRPA provides the essential improvement over the Hartree-Fock theory (a nonrelativistic mean-field theory) in obtaining good-quality xenon wave functions of not only the ground state but also excited states.

* In our previous many-body calculations for germanium atoms [12], we need one extra feature, the multiconfiguration ground state, to handle open-shell atoms properly. The method was given the name: multiconfiguration random phase approximation (MCRPRA) by its early pioneers [13, 16].

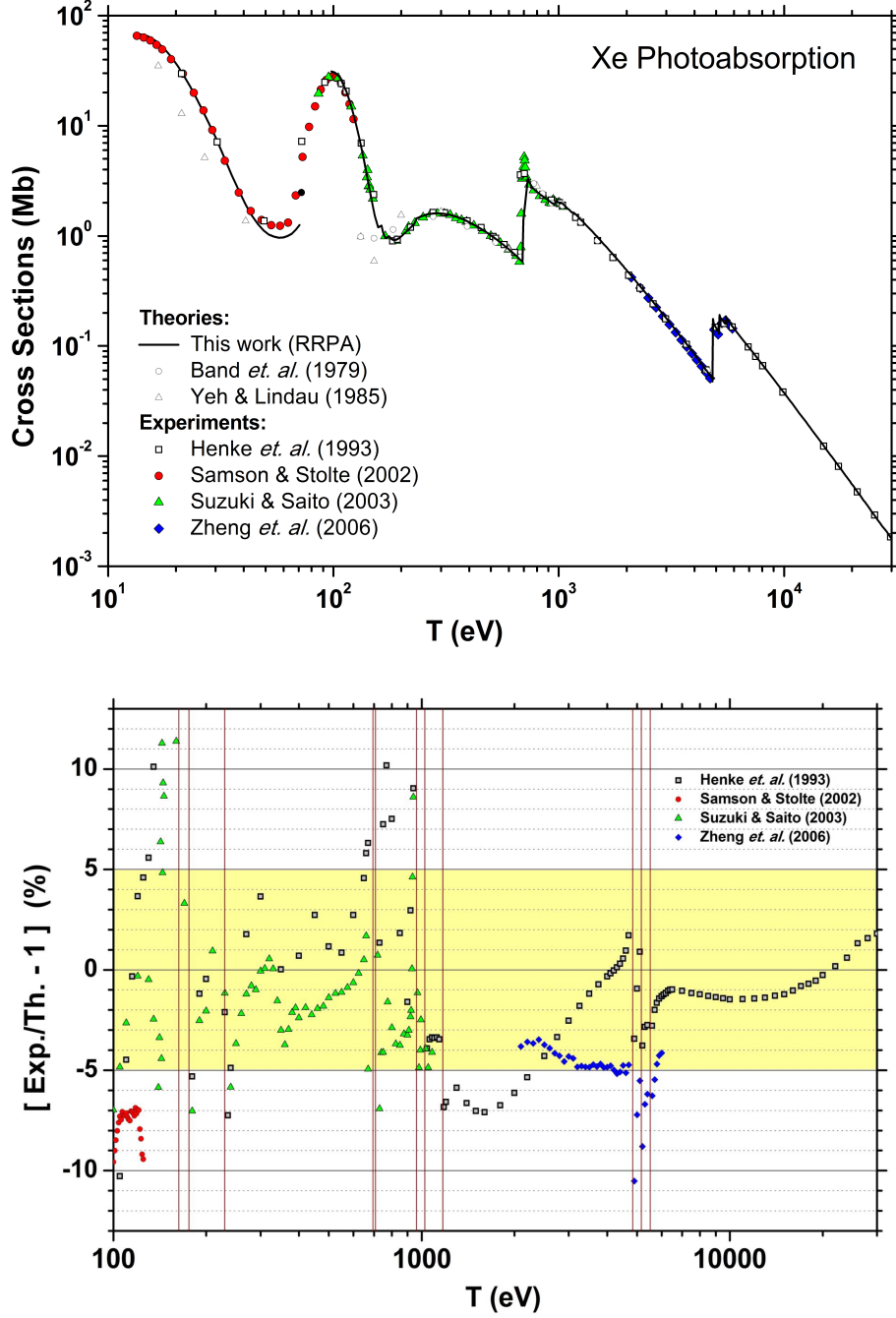


FIG. 1. (Top) Photoabsorption cross section of Xe. The black solid line shows the results of our RRPA calculation. Points in empty squares and colors are experimental data compiled from Refs. [17–20], and points in empty circles and triangles are theory predictions [21, 22]. (Bottom) The relative difference between our RRPA calculation and experimental data.

Benchmark calculations for our atomic many-body calculations of xenon were done in two steps. First we compare in Table I all the single-particle energies calculated by the Dirac-Hartree-Fock (DHF) theory with the edge energies extracted from photoabsorption data accumulated before 1990 [17]. Except for a few intermediate shells including N_I , N_{II} , N_{III} , and O_I , the general agreement

is good.

Second, we calculate the total cross section of photoabsorption σ_γ , which is dominated by photoionization for photon energy ranging between 12.1 eV (the ionization threshold) and 30 keV. Our result is shown as the black solid line in the top panel of Fig. 1 and is compared with experimental data compiled from Refs. [17–20]. The computation does not converge well between 70–100 eV, so it is left empty in this range except the black point just above 70 eV. Our result visibly deviates from data between 40–70 eV, but generally agrees with data well across more than four orders of magnitude in cross section. Two previous theory predictions [21, 22] are also shown in this panel by empty circles and triangles, respectively. In comparison, our calculation consistently works better in this broad energy range considered.

More detailed comparison between different sets of data and our result is shown in the bottom panel of Fig. 1. The data have at least $\sim 2 - 5\%$ (1 sigma) errors which are not shown here. In most region, the difference is less than 5%. Larger differences could happen near ionization thresholds of atomic shells (indicated by vertical lines), but they do not give significant contributions when a broad range of spectrum is integrated. Therefore, we can assign a conservative averaged theory error of 5% to our calculation in the energy range of $100 \text{ eV} \leq T \leq 30 \text{ keV}$. If one only considers the energy range between 2–30 keV, the averaged error is further reduced to 2–3%.

IV. RESULTS AND DISCUSSION

Taking confidence on the xenon wave functions obtained by our many-body approach, the neutrino-ionization process is computed as outlined in Eqs. (1–4) in the energy range of $100 \text{ eV} \leq T \leq 30 \text{ keV}$.

For solar neutrino flux, we consider two main sources: the proton-proton fusion, $p+p \rightarrow d+e^++\nu_e$ (the pp neutrinos), and the electron capture by ${}^7\text{Be}$, ${}^7\text{Be} + e^- \rightarrow {}^7\text{Li} + \nu_e$ (the ${}^7\text{Be}$ neutrinos). The former has a continuous spectrum ended at 420 keV; the latter has two discrete spectral lines: one at 862 keV and the other at 384 keV with branching ratios 89.6% and 10.4%, respectively. Together they amount to 98% of the total solar neutrino flux.

The fluxes of the pp and ${}^7\text{Be}$ neutrinos

$$\phi_{pp} = 5.98 \times 10^{10} \text{ cm}^{-2} \text{ s}^{-1}, \quad \phi_{{}^7\text{Be}} = 5.00 \times 10^9 \text{ cm}^{-2} \text{ s}^{-1}, \quad (6)$$

are taken from the recent Standard Solar Model (SSM) prediction in [23], which incorporated updated nuclear reaction rates in [24].[†] The spectral shape of the pp neutrinos is approximated by the standard

[†] The pp and ${}^7\text{Be}$ neutrino fluxes adopted in [7] is from an earlier SSM prediction [25]; both are somewhat smaller than the ones of [23].

β -decay form

$$\frac{d\phi_{pp}^{(e)}(E_\nu)}{dE_\nu} = A(Q + m_e - E_\nu)[(Q + m_e - E_\nu)^2 - m_e^2]^{\frac{1}{2}} E_\nu^2 F, \quad (7)$$

where the Q -value is 420 keV, the Fermi function $F \cong 1$, and the normalization factor $A = 2.97 \times 10^{-36} \text{ keV}^{-2}$ is fixed by the chosen pp flux $\phi_{pp}^{(e)}$ above.[‡]

The flavor content of solar neutrinos seen in terrestrial detectors is modified by neutrino oscillation both in vacuum between the Earth and the surface of the Sun, and in medium between the solar surface and core by the Mikheyev-Smirnov-Wolfenstein (MSW) effect. Current observations of low-energy solar neutrinos including pp and ${}^7\text{Be}$ are consistent with the MSW–large-mixing-angle (MSW-LMA) solution: It predicts a vacuum-dominated oscillation pattern and the survival probability of electron neutrinos can be approximated as [27]

$$P_{ee} = \cos^4 \theta_{13} \left(1 - \frac{1}{2} \sin^2(2\theta_{12}) \right) + \sin^4 \theta_{13}. \quad (8)$$

Using the most recent oscillation angles recommended by the Particle Data Group: $\sin^2(2\theta_{12}) = 0.846 \pm 0.021$ and $\sin^2(2\theta_{13}) = 0.085 \pm 0.005$ [28], $P_{ee} = 0.553$ with an error about 2%. The remaining part of the pp and ${}^7\text{Be}$ fluxes contains either ν_μ or ν_τ , and scatters with the same differential cross section formula $d\sigma^{(\mu)}/dT = d\sigma^{(\tau)}/dT$.

In Fig. 2, we show our flux-averaged ν_e -Xe differential cross sections (in solid lines) for electron neutrinos of pp , ${}^7\text{Be}(862 \text{ keV})$, and ${}^7\text{Be}(384 \text{ keV})$, respectively. The general trends of $\langle d\sigma/dT \rangle$ show little dependence on neutrino sources, and its functional behavior is largely controlled by the value of T and the binding energies of atomic shells (indicating by the vertical thin lines). The former determines the number of electrons that can be ionized, and the latter gives those sharp edges indicating large differential cross sections whenever an atomic shell is just open. In combination, the largest value of $\langle d\sigma/dT \rangle$ is reached at $T \sim 5 \text{ keV}$, which corresponds to the opening of L shells of xenon.

The dashed lines in this figures are the predictions of the stepping approximation

$$\frac{d\sigma^{(i)}}{dT} = \sum_{i=1}^Z \theta(T - B_i) \frac{d\sigma_0^{(i)}}{dT}. \quad (9)$$

This is done by weighting the scattering cross section of a neutrino and a free electron, $d\sigma_0/dT$, with the number of electrons that can be ionized by an energy deposition of T , where θ is the step function and B_i is the binding energy of the i th electron. It is clearly shown in these figures that the atomic binding suppresses the cross sections, similar to our previous work on the germanium atom.

[‡] The pp flux is peaked within 100-400 keV in neutrino energy. This simple parametric form agrees within 1% with the more sophisticated one derived from an explicit solar model calculation [26] for $E_\nu \gtrsim 10 \text{ keV}$.

Note that in this plot of $\langle d\sigma/dT \rangle$ we do not try to join the points at low recoil energies, $T \lesssim 250$ eV. This reflects a numerical difficulty of obtaining stable solutions near the low-energy edges. In general, one can expect a sharp increase in $\langle d\sigma/dT \rangle$ when an atomic shell is just open, and use the stepping approximation prediction to set a upper bound. For more reliable predictions from detailed many-body calculations, we shall leave them to future studies.

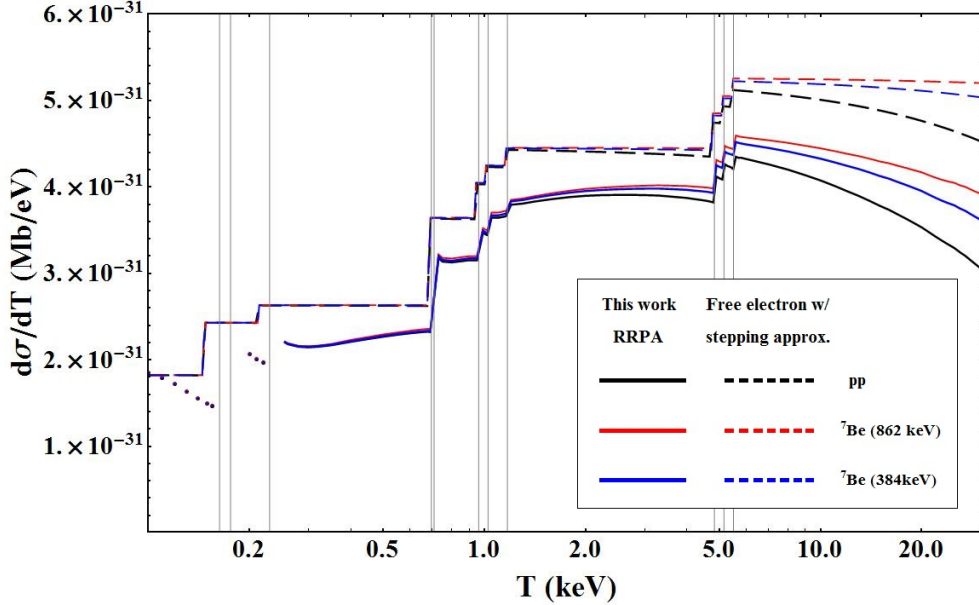


FIG. 2. Flux-averaged differential cross sections of xenon ionization by electron neutrinos from pp , ${}^7\text{Be}(862\text{ keV})$, and ${}^7\text{Be}(384\text{ keV})$ sources in solid black, red, and blue lines, respectively. The dashed lines are the predictions of the stepping approximation (see text for more details).

Finally we present in Fig. 3 the differential count rate of electronic recoil induced by solar neutrinos in a xenon detector of one-ton mass and one-year exposure and assuming a 99.98% event rejection [5]. (Other rejection levels of 99.6% [29] and 99.987% [30] are used for discussion in Ref. [31]). The energy range, 100 eV–30 keV is fixed by the threshold of detecting electronic recoil at the low end[§] and the dominance of the $2\nu\beta\beta$ decay background from ${}^{136}\text{Xe}$ (the dotted blue line) at the high end. Compared with Ref. [5], which used a naive free electron approximation without stepping (i.e., all 54 electrons of xenon contribute regardless of T), our calculation show a consistent suppression due to atomic binding (the red vs. the blue line). Also shown are two cases of WIMP induced nuclear recoil (with DARWIN detector parameters) translated into electron equivalent energy to show that solar neutrino background becomes the limiting factor in these scenarios. The $2\nu\beta\beta$ and WIMP curves all taken from Ref. [5].

[§] We thank H. Nelson for pointing to us this low threshold of xenon detectors in electronic recoil.

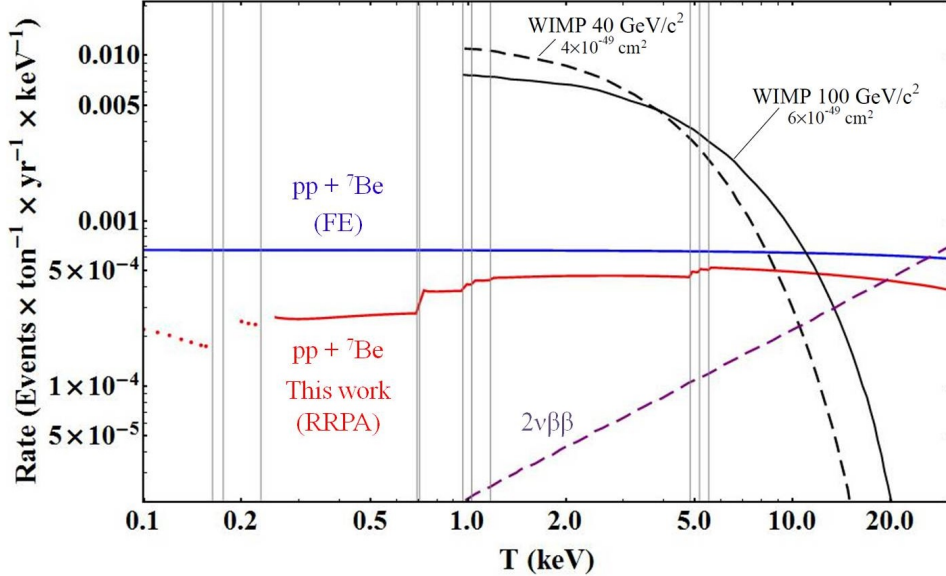


FIG. 3. Differential count rate of electronic recoil induced by solar neutrinos in xenon detectors assuming a 99.98% rejection. The red line is our RRPA result and the blue line is the free electron approximation without stepping function as adopted in Ref. [5]. Also shown are another neutrino background from the two-neutrino double β decay ($2\nu\beta\beta$) of ^{136}Xe and two cases of WIMP induced nuclear recoil (with DARWIN detector parameters) translated into electron equivalent energy. The $2\nu\beta\beta$ and WIMP curves all taken from Ref. [5].

In Table II, we compare our predictions of solar neutrino induced event rates, assuming a 1-ton-year exposure, with the ones of the free electron (FE) approximation without stepping functions introduced, as adopted in Refs. [5, 7].[¶] Using this as a channel for low energy solar neutrino detection, the atomic binding effect reduces the event rates in the energy window of 2-30 keV by 28% and 24% respectively for pp and ^7Be neutrinos. This causes a huge loss of statistics that is required for checking the standard solar model prediction of low-energy solar neutrino fluxes at 1% level. On the other hand, our theoretical calculation is benchmarked with an error estimate at 2 – 3% level, which is just slightly larger than the desired goal, so the experimental data can be interpreted without this theoretical uncertainty under good control. As for this channel being a potential background in WIMP searches, the suppression due to atomic binding turns out to be a good news: It implies the sensitivity to WIMP-nucleon cross section is increased by a similar factor, unless the rejection of electronic recoil can reach an even higher level such that this background becomes subdominant

[¶] We note that our FE results differ slightly from Refs. [5, 7] due to different mixing parameters, neutrino fluxes, etc.

being used. Also we would like to point out a typographical error in Eq.(2.5) of Ref. [7]: the last term should be $gLgR \frac{m_e T}{E_\nu^2}$.

TABLE II. Comparison of solar neutrino induced event rates predicted by our many-body calculations (RRPA) and the free electron (FE) approximation without stepping functions (as adopted by Refs. [5, 7]) for a xenon detector with 1-ton-year exposure.

Physics channel	Low-energy ν measurement			Dark matter search		
Energy range	2–30 keV			2–10 keV		
Assumptions	No ER/NR discrimination			99.98% ER rejection, 30% NR acceptance		
Model	FE	RRPA	Diff.	FE	RRPA	Diff.
Solar pp neutrinos	80.7	57.8	–28%	4.8×10^{-3}	3.6×10^{-3}	–25%
Solar ${}^7\text{Be}$ neutrinos	7.1	5.4	–24%	4.1×10^{-4}	3.2×10^{-4}	–23%
Total	87.8	63.2	–28%	5.2×10^{-3}	3.9×10^{-3}	–24%

compared to the one from coherent neutrino-nucleus scattering.

V. SUMMARY

The importance of low-energy electronic recoil induced by solar neutrinos in multi-ton xenon detector is two-fold: On one hand, it is a background that should be properly removed in searches of WIMP-nucleus scattering. On the other hand, it provides a viable channel to detect solar pp and ${}^7\text{Be}$ in “real time” [5] and has the potential to measure their fluxes at the precision level of standard solar model predictions. In this work, we have applied an *ab initio* many-body method: the relativistic random phase approximation (RRPA) to this problem with good benchmarks from xenon structure and photoabsorption data. We have also presented the electronic recoil rate spectrum in the energy window of 100 eV – 30 keV with the standard per ton per year normalization for xenon detectors. Except small regions near ionization thresholds of atomic shells, we estimate our theoretical error less than 5% in general, and the averaged error in the energy window of 2–30 keV only 2–3%, which is just slightly larger than the precision level ($\sim 1\%$) of the current solar models. We found that the atomic binding effect yields a sizable suppression to the neutrino-electron scattering cross section at low recoil energies in xenon detectors. Compared with the previous calculation based on the free electron picture, our calculated event rate of electronic recoil in the same detector configuration is reduced by about 30%. This increases the demand of detector volume and/or exposure time for precision measurements of solar neutrino fluxes. However, it also increases the sensitivity to WIMP-nucleon scattering cross section.

ACKNOWLEDGMENTS

We thank Dr. Harry Nelson (UCSB) for bringing this interesting problem to our attention and useful discussions. We also thank Chih-Liang Wu for early involvement in this project. This work is supported in part by the Ministry of Science and Technology, Taiwan under Grants Nos. 105-2112-M-002-017-MY3 and 105-2918-I-002-003 (J.-W. C. and C.-P. W.), 104-2112-M-259-004-MY3 (C.-P. L.); the National Center for Theoretical Sciences; the Center for Theoretical Sciences and Center of Advanced Study in Theoretical Sciences of National Taiwan University (J.-W. C. and C.-P. W.); and MIT MISTI program (J.-W. C. and C.-P. W.).

-
- [1] A. Tan *et al.* (PandaX-II), *Phys. Rev. Lett.* **117**, 121303 (2016), arXiv:1607.07400 [hep-ex].
 - [2] D. S. Akerib *et al.*, (2016), arXiv:1608.07648 [astro-ph.CO].
 - [3] E. Aprile *et al.* (XENON), *JCAP* **1604**, 027 (2016), arXiv:1512.07501 [physics.ins-det].
 - [4] D. S. Akerib *et al.* (LZ), (2015), arXiv:1509.02910 [physics.ins-det].
 - [5] J. Aalbers *et al.* (DARWIN), (2016), arXiv:1606.07001 [astro-ph.IM].
 - [6] J. Billard, L. Strigari, and E. Figueroa-Feliciano, *Phys. Rev. D* **89**, 023524 (2014), arXiv:1307.5458 [hep-ph].
 - [7] L. Baudis, A. Ferella, A. Kish, A. Manalaysay, T. Marrodan Undagoitia, *et al.*, *JCAP* **1401**, 044 (2014), arXiv:1309.7024 [physics.ins-det].
 - [8] G. Bellini *et al.* (BOREXINO Collaboration), *Nature* **512**, 383 (2014).
 - [9] G. Bellini *et al.*, *Phys. Rev. Lett.* **107**, 141302 (2011), arXiv:1104.1816 [hep-ex].
 - [10] J.-W. Chen, H.-C. Chi, K.-N. Huang, C.-P. Liu, H.-T. Shiao, *et al.*, *Phys. Lett. B* **731**, 159 (2014), arXiv:1311.5294 [hep-ph].
 - [11] J.-W. Chen, H.-C. Chi, H.-B. Li, C. P. Liu, L. Singh, H. T. Wong, C.-L. Wu, and C.-P. Wu, *Phys. Rev. D* **90**, 011301 (2014), arXiv:1405.7168 [hep-ph].
 - [12] J.-W. Chen, H.-C. Chi, K.-N. Huang, H.-B. Li, C.-P. Liu, L. Singh, H. T. Wong, C.-L. Wu, and C.-P. Wu, *Phys. Rev. D* **91**, 013005 (2015), arXiv:1411.0574 [hep-ph].
 - [13] W. R. Johnson and C. D. Lin, *Phys. Rev. A* **20**, 964 (1979).
 - [14] W. R. Johnson and K. T. Cheng, *Phys. Rev. A* **20**, 978 (1979).
 - [15] K.-N. Huang, W. R. Johnson, and K. T. Cheng, *At. Data Nucl. Data Tables* **26**, 33 (1981).
 - [16] K.-N. Huang and W. R. Johnson, *Phys. Rev. A* **25**, 634 (1982).
 - [17] B. L. Henke, E. M. Gullikson, and J. C. Davis, *Atom. Data Nucl. Data Tables* **54**, 181 (1993).

- [18] J. Samson and W. Stolte, *J. Electron Spectrosc. Relat. Phenom.* **123**, 265 (2002).
- [19] I. H. Suzuki and N. Saito, *J. Electron Spectrosc. Relat. Phenom.* **129**, 71 (2003).
- [20] L. Zheng, M. Cui, Y. Zhao, J. Zhao, and K. Chen, *J. Electron Spectrosc. Relat. Phenom.* **152**, 143 (2006).
- [21] M. Band, Y. I. Kharitonov, and M. B. Trzhask-Ovskaya, *At. Data Nucl. Data Tables* **23**, 443 (1979).
- [22] J. J. Yeh and I. Lindau, *At. Data Nucl. Data Tables* **32**, 1 (1985).
- [23] A. M. Serenelli, W. C. Haxton, and C. Pena-Garay, *Astrophys. J.* **743**, 24 (2011), arXiv:1104.1639 [astro-ph.SR].
- [24] E. G. Adelberger *et al.*, *Rev. Mod. Phys.* **83**, 195 (2011), arXiv:1004.2318 [nucl-ex].
- [25] J. N. Bahcall, A. M. Serenelli, and S. Basu, *Astrophys. J.* **621**, L85 (2005), arXiv:astro-ph/0412440 [astro-ph].
- [26] J. N. Bahcall, *Phys. Rev. C* **56**, 3391 (1997), arXiv:hep-ph/9710491 [hep-ph].
- [27] J. N. Bahcall and C. Pena-Garay, *New J. Phys.* **6**, 63 (2004), arXiv:hep-ph/0404061 [hep-ph].
- [28] K. A. Olive *et al.* (Particle Data Group), *Chin. Phys. C* **38**, 090001 (2014).
- [29] D. S. Akerib *et al.* (LUX), *Phys. Rev. Lett.* **112**, 091303 (2014), arXiv:1310.8214 [astro-ph.CO].
- [30] D. Yu. Akimov *et al.*, *Phys. Lett.* **B709**, 14 (2012), arXiv:1110.4769 [astro-ph.CO].
- [31] M. Schumann, L. Baudis, L. Bütikofer, A. Kish, and M. Selvi, *JCAP* **1510**, 016 (2015), arXiv:1506.08309 [physics.ins-det].